frontiers in Geochemistry

TYPE Original Research
PUBLISHED 12 March 2026
DOI 10.3389/fgeoc.2026.1766699

OPEN ACCESS

EDITED BY
Maria Aurora Armienta,
National Autonomous University of Mexico, Mexico

REVIEWED BY
Victor Fonabe Embui,
Institut de Recherches Géologiques et Minières (IRGM), Cameroon
Ayşe Orhan,
Nevsehir University, Türkiye

*CORRESPONDENCE
Rute Salgueiro,
rute.salgueiro@lneg.pt

RECEIVED 12 December 2025
REVISED 30 January 2026
ACCEPTED 02 February 2026
PUBLISHED 12 March 2026

CITATION
Salgueiro R, Silva TP, Martín-Méndez I, de Oliveira D, Batista MJ and Inverno C (2026) Insights into rare earth elements and other critical raw materials from Castelo Branco massif alluvial deposits (Portugal).
Front. Geochem. 4:1766699.
doi: 10.3389/fgeoc.2026.1766699

Insights into rare earth elements and other critical raw materials from Castelo Branco massif alluvial deposits (Portugal)

Rute Salgueiro[1]*, Teresa Pena Silva[1], Iván Martín-Méndez[2], Daniel de Oliveira[1], Maria João Batista[1] and Carlos Inverno[1]

[1]Unidade de Recursos Minerais e Geofísica, Laboratório Nacional de Energia e Geologia, Amadora, Portugal, [2]Departamento de Recursos Geológicos para la Transición Energética, CN Instituto Geológico y Minero de España (IGME-CSIC), Madrid, Spain

Actual and future demands for critical raw materials and strategic raw materials (CRM/SRM) justify the global search for their potential sources and the exploration approaches to reach them. This study discloses the characterization of rare earth elements (REE) and other CRM-bearing alluvial heavy minerals samples sourced from the late- to post-tectonic Variscan Castelo Branco Massif (Portugal). It also contributes to an understanding of REE, Th, and U anomalies from local and correspondent stream sediments identified in past geochemical surveys. The alluvial samples were subjected to semiquantitative analysis of their minerals under a binocular microscope and to chemical analysis through portable X-ray fluorescence. A varied mineralogical association and a geochemical fingerprint compatible with their main granitic source was identified, revealing several minerals that carry CRM, in which REE and titanium minerals stood out. The titanium minerals have the higher average abundance (54%), being ilmenite-dominant (50%), as supported by the relatively higher Ti content of these samples (up to 28.88%). The REE minerals occur as accessories and have a summing average of 12%, in which monazite is the most abundant (4.97%). Geochemical data support alluvial monazite as the mineral with the highest REE and Th concentrations, as described in the literature on its granitic source. In addition, the magnetic fraction of samples (~85%) that includes monazite and xenotime presents LREE anomalous contents (up to 4,557 mg/kg) in relation to their granitic source, NASC, and even to ΣREE anomalous values revealed by local stream sediments. The Th (up to 1,969 mg/kg) and U (up to 244 mg/kg) contents follow the same trend. Nevertheless, the nonmagnetic mineral fraction that includes apatite and zircon reaches higher U contents (up to 448 mg/kg). This study indicates that the SRM Ti (ilmenite) and LREE (monazite) have the potential to form placer deposits sourced from Castelo Branco granitic rocks in a wider area, which is supported by the regional Ti placers exploited in the past. The occurrence of other accessory elements/minerals with industrial applicability associated with those placers may also represent future added value.

KEYWORDS
alluvial heavy minerals, CRM, ilmenite, mineral exploration, monazite, REE, SRM, xenotime

1 Introduction

Critical raw materials (CRM) are fundamental to progressive economies and the EU's green digital transition (European Commission, 2021). In 2023, the European Commission identified and published a list of 34 CRM and for the first time introduced 17 strategic raw materials (SRM) (European Commission, 2023). Most (15) of these SRM are also considered CRM: bismuth, gallium, battery-grade manganese, rare earth elements (REE) for magnets, metallurgy-grade boron, germanium, battery-grade natural graphite, silicon metal, cobalt, battery-grade lithium, titanium metal, magnesium metal, platinum group metals, and tungsten. The remaining two SRM, copper and nickel, are not considered critical (European Commission, 2023) (https://rmis.jrc.ec.europa.eu/eu-critical-raw-materials). The worldwide demand for CRM is increasing, and Europe is highly dependent on imports. To reduce this vulnerability, the European commission adopted Regulation (EU) 2024/1252 (*Raw Materials Act*) to ensure sustainable supply and diversify value chains to support its 2030 climate and digital European targets (European Commission, 2024). This growing demand has boosted geological exploration and a reassessment of areas with potential REE mineralization. Beyond the designated CRM and SRM, several other elements and minerals are frequently used as industrial commodities (e.g., Sn and Zr) or minerals (e.g., cassiterite, zircon, ilmenite and rutile) in the global market (Subasinghe et al., 2022). This necessarily drives the exploration, (re) assessment, and research of areas with potential in these elements.

REE ore deposits can be genetically associated with endogenous (magmatic or hydrothermal) and exogenous (sedimentary and/or climatic) geological processes (Charles et al., 2023 and references therein). In Europe, the main known resources of REE are associated with the aforementioned processes in alkaline complexes and carbonatites (Goodenough et al., 2016). Nevertheless, there are some other REE-bearing deposits associated with exogenous processes, such as placers in Greek, French, German, and Spanish sedimentary basins (Charles et al., 2023 and references therein). In REE-bearing deposits, as in many other ore deposits, the ore minerals are part of the heavy minerals (HM) group—that is, according to Morton (1978), minerals with a density >2.8–2.9 g/cm^3—and, specifically, in these cases are monazite, xenotime, allanite, and euxenite (Balaram, 2022). Both rocks and stream sediments, as well as alluvial sediments, contain natural concentrations of HM. Weathering is an important natural process that enhances the concentration of REE in surface environments, leading to the formation of distinct secondary CRM ore deposits such as placers, laterites, and ion-adsorption clays (Balaram, 2022). Among these, granitic rocks contain in their composition industrial HM, which contain CRM. Consequently, the dismantling of source protoliths contributes to the enrichment of valuable minerals in the sedimentary cycle, trapped in alluvial deposits. In some cases, these mineral concentrations reach economic importance, forming placers that can be exploited. In Portugal, the Laboratório Nacional de Energia e Geologia (LNEG) and its predecessors have conducted extensive research and exploration of CRM (-bearing) minerals within alluvial heavy mineral deposits (Inverno et al., 1998; Lencastre, 1999; Inverno et al., 2007; Rosa et al., 2010; Salgueiro et al., 2010; Salgueiro et al., 2014; Salgueiro et al., 2015; Salgueiro et al., 2020). In the Vale da Silveira, on the eastern edge of the Castelo Branco Massif (CBM), REE, U, and Th anomalies in stream sediments draining from granitic facies affected by late NE–SW faults were identified (Inverno et al., 2007). Sn-Ti placers associated with the granitic rocks of this region are also known (Sanches et al., 2012; Antunes et al., 2014; SIORMINP, 2025). Therefore, the Vale de Silveira geological environment contains some mineral potential for the occurrence of both REE and other CRM/SRM in alluvial deposits. The aim of this study was to identify, using binocular microscope and portable XRF (pXRF), chemical composition data on alluvial HM samples, with a focus on REE and other CRM. Using these two simple methodologies, this study also contributes to better understand the origin of the stream sediment REE(t), U, and Th anomalies identified in this area by Inverno et al. (2007) and highlights the potentially economic CRM value of alluvial/placer deposits over CBM outcrops.

2 Geological setting

The present study focuses on alluvial samples collected from Vale da Silveira (Castelo Branco district, central Portugal) in the tectono-stratigraphic Central Iberian Zone (CIZ; Figure 1). The granitic rocks in this region belong to the east border of the peraluminous affinity (late- to post-tectonic) Variscan CBM, which outcrops for over 390 km^2 (Antunes, 2006; Antunes et al., 2008; Antunes et al., 2014; Antunes et al., 2011). Oliveira et al. (1992) distinguished three concentric granitic facies in this massif: muscovite-biotite granite (fine grained) in the core and (coarse grained) porphyritic in the border, and monzonitic granites (with sparse megacrystals) and porphyritic monzonitic granites in the middle (Figure 1). Recent studies have classified this massif structure as five concentric S-type granitic facies rather than the previous three, with U–Pb–Th ages ranging from 303 ± 3 Ma to 297 ± 3 Ma (Antunes, 2006; Antunes, 2014), and ID-TIMS U–Pb ages for zircon and monazite pointing to a pluton formation at 310 ± 1 Ma (Antunes et al., 2008). The sample sites of the present study occur in alluvia over the monzonitic porphyritic granites, according to the classification of Oliveira et al. (1992) mentioned above (Figure 1), and over biotite-muscovite granodiorite porphyry and two mica granite facies, according to the classification of Antunes (2006). The HM assemblage reported for granitic rocks includes ilmenite, tourmaline, monazite, zircon, apatite, biotite, muscovite, rutile, andalusite, sillimanite and rare allanite, and sphene (Antunes, 2006; Antunes et al., 2008). Nevertheless, according to Antunes et al. (2008), biotite is subordinated to muscovite in the core and border muscovite–biotite granites, contrasting with pluton middle facies where biotite is equal or dominant over muscovite near the core facies. Zircon and monazite occur mainly as inclusions in apatite, biotite, and plagioclase. Ilmenite, which is the most abundant opaque mineral and is present in all the granitic facies, is mainly included in biotite and is disseminated in the rock (Antunes, 2006). Geochemical data show that the middle granitic facies, especially the monzonite granite nearest the core, are enriched

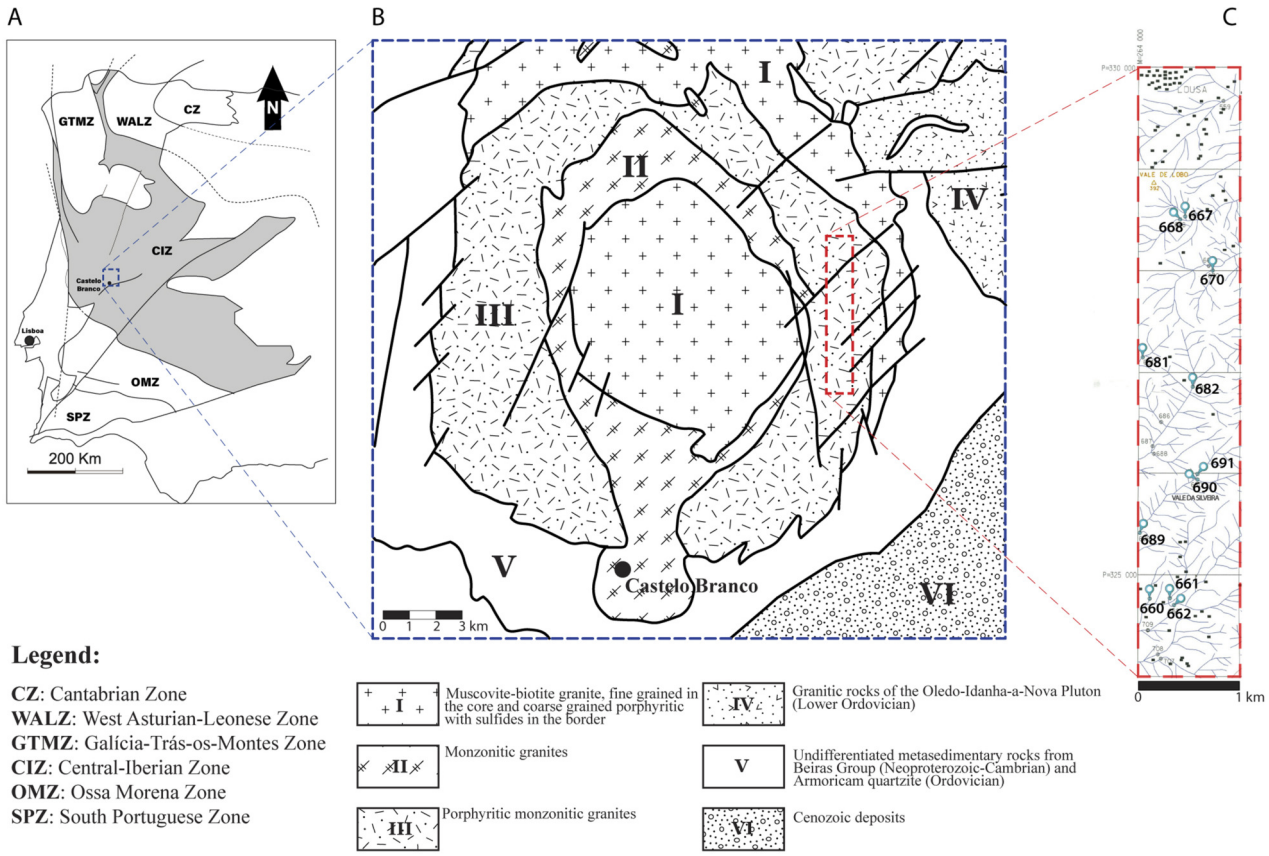

FIGURE 1
(A) Geotectonic map of the Iberian Massif (adapted from Gaspar et al., 2022) showing the region of the study area within blue dashed lines. **(B)** Geological setting map of the study area region (adapted from Oliveira et al., 1992); **(C)** Alluvial sampling sites (adapted from Inverno et al., 2007).

in REE in relation to core and border muscovite–biotite granites (Antunes et al., 2008). Emplacement of the granitic rocks occurred by intruding the Neoproterozoic–Cambrian Beiras Group metasediments, composed of fine turbidites and conglomerates and promoting the development of a contact metamorphic aureole up to 2 km wide in these rocks. Metasedimentary xenoliths and surmicaceous enclaves were identified in the granitic rocks (Antunes et al., 2008). The ore mineralization known in this region includes the cassiterite and ilmenite Lardosa alluvial placer deposits exploited in the CBM from 1980 to 1988 (Sanches et al., 2012; Antunes et al., 2014; SIORMINP, 2025), for which the formation is a consequence of the erosion of the muscovite-biotite granite in the CBM border (Iglesias et al., 2020). Other Sn-Ti placers occur in the area between the muscovite–biotite granite in the core and monzonitic granite with sparse megacrystals of the same batholith (SIORMINP, 2025). Ilmenite is part of the HM assemblage of the CBM rocks and cassiterite is sourced from intragranitic Sn-W mineralized quartz veins (Antunes, 2020; Antunes, 2006; Sanches et al., 2012; SIORMINP, 2025) that fill late to post-tectonic Variscan faults that strike NW–SE to WNW–ESE (Antunes et al., 2014; SIORMINP, 2025). Additionally, several late tectonic fault structures, NE–SW and N–S oriented, cut across granitic and metasedimentary rocks (Figure 1; Oliveira et al., 1992; Antunes, 2006).

3 Materials and methods

The 12 selected alluvial samples for the present study were sourced from granitic terrains located near the eastern CBM border (Figures 1B,C) and around late NE–SW tectonic faults where, according to Inverno et al. (2007), the stream sediments reveal anomalous REE concentrations. The samples were sieved (<3 mm) and panned in the field. In the laboratory, after drying, the HM were isolated using heavy liquids (2.89 g/cm^3) and then separated by magnetic susceptibility, producing two mineral fractions: a) magnetic and paramagnetic minerals, referred to as the "magnetic fraction" (MG), and b) diamagnetic minerals, referred to as the "non-magnetic fraction" (NM). The two mineral fractions obtained for each sample were analyzed individually under a binocular microscope. For the semi-quantification of each mineral in relation to the volume of the respective mineral fraction, the following range values were used: <1% (V; lower limit considered 0.01%), 1%–5% (R), 5%–25% (P), 25%–50% (Md), 50%–75% (A), and 75%–100% (M) (adapted from Parfenoff et al., 1970). Mineral average percentage determination

TABLE 1 Mineralogical identification and semi-quantification analysis under binocular microscope of minerals present in each mineral fraction, magnetic (magnetic and paramagnetic minerals) and nonmagnetic (diamagnetic minerals), for the 12 alluvial samples from Vale da Silveira (Castelo Branco). V: <1%; R: 1%–5%; P: 5%–25%; Md: 25%–50%; A: 50%–75%; M: 75%–100% (adapted from Parfenoff et al., 1970).

Magnetic mineral fraction (MG)										
Monazite	Xenotime	Epidote group	Ilmenite	Sphene	Tourmaline	Garnet	Leucoxene (MG)	Biotite	Iron oxy./hydroxides	Volume (cm^3)
P	V	V	A	—	Md	P	V	P	R	2.8
P	V	R	A	—	P	—	—	P	V	2.8
P	V	V	A	—	P	R	V	P	V	1.1
V	V	V	A	—	P	R	—	P	V	6.4
V	V	V	A	—	R	R	—	R	V	8.5
V	V	V	M	—	P	R	V	R	V	7.1
V	V	V	A	—	P	R	—	Md	R	1.4
P	V	—	A	—	P	V	—	P	—	1.8
R	V	R	A	—	P	P	—	R	—	2.8
V	—	V	Md	—	R	R	V	V	V	5.7
V	V	V	M	V	P	R	V	R	V	2.1
P	R	P	A	—	P	P	—	P	—	4.2

Nonmagnetic mineral fraction (NM)													
Scheelite	Apatite	Zircon	Cinnabar	Rutile	Anatase	Brookite	Andalusite	Kyanite	Sillimanite	Leucoxene (NM)	Muscovite	Topaz	Volume (cm^3)
V	Md	P	—	V	P	—	Md	—	—	V	V	R	0.71
—	P	P	—	—	P	—	A	—	R	—	—	R	0.71
V	P	P	—	R	P	V	Md	—	V	V	V	V	0.71
V	P	P	—	—	P	—	P	V	P	—	V	R	0.71
V	Md	P	V	P	P	V	Md	V	R	—	V	V	0.71
V	P	P	—	V	P	—	P	—	—	V	V	P	0.71
V	A	R	—	—	P	—	—	V	P	V	V	R	0.71
—	P	P	V	R	P	—	P	—	V	—	—	V	0.71
V	—	P	V	—	P	—	Md	—	V	V	V	—	0.71
V	P	P	—	V	Md	—	Md	—	—	V	V	P	0.71
—	—	P	V	P	P	V	Md	—	R	—	V	R	0.71
—	P	P	V	P	P	V	P	—	—	—	—	—	0.71

10.3389/fgeoc.2026.1766699

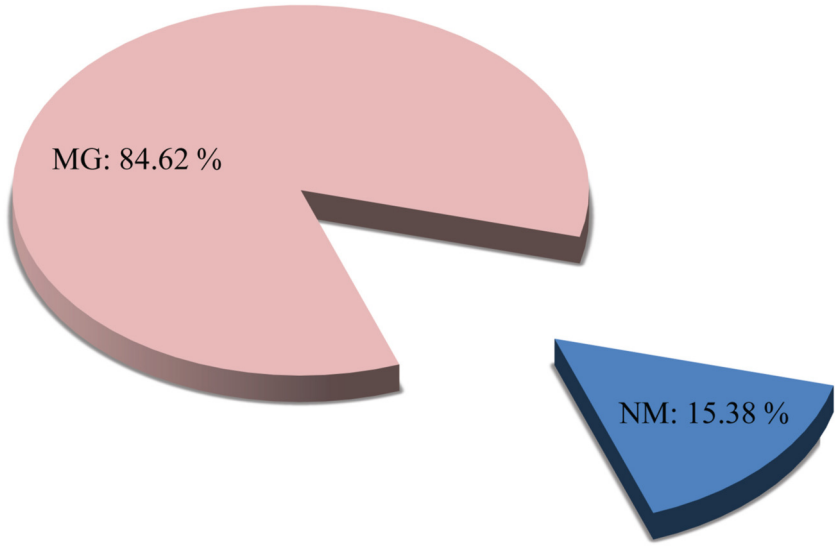

FIGURE 2
Representative diagram with the total volume (in percentage) of mineral fractions (MG: magnetic and NM: nonmagnetic) from the 12 alluvial heavy mineral samples from Vale da Silveira (Castelo Branco).

was obtained using the average value of each range described above (e.g., for Md: 37.5%) and the total volume of the sample (MG + NM). Scheelite was identified using ultraviolet light (UV). Both alluvial HM fractions of the 12 samples were subjected to chemical analysis using the portable X-ray fluorescence (pXRF) equipment X-MET8000 Expert Geo from HITACHI (Tokyo, Japan) in the laboratory, connected to a benchtop stand. This apparatus was equipped with a Rh tube (4 W) and a silicon drift detector (SDD). Two analytical programs (calibrations) were used: Mining (40 kV, 120 s per sample) and REE (for La, Ce, Pr, and Nd during 180 s, 50 kV). To overcome the difficulty of measuring the samples in the form of mineral grains, eight measurements were performed on each sample, and the sample holder was shaken between essays. The average of the results was then considered. It is important to note that these samples could not be ground, since their purpose was to be studied further, counting on the original physical and textural characteristics of the mineral grains.

4 Results

4.1 Mineralogical characterization of alluvial heavy mineral concentrates

The results in Table 1 and Figure 2 indicate that the MG of the set of the studied twelve alluvial HM concentrates presented a higher volume (~85%) than the NM (~15%), meaning that the representativeness of the minerals from the MG will be relatively higher than those from the NM. The results of the semi-quantification analysis under binocular microscope are presented in Table 1, where the identified mineral assemblage of the two mineral fractions (MG and NM) is listed for each sample. The most representative minerals from the MG are ilmenite [(Fe, Mg, Mn, Zn)TiO_3; up to 75%–100%], tourmaline ([Na(Mg, Fe, Mn, Li, Al)$_3$ Al_6 [Si_6 O_{18}](BO_3)$_3$ (O,OH,F)$_4$]; up to 25%–50%), monazite [(Ce, LREE, Th, U, Ca)PO_4; up to 5%–25%], biotite [K(Mg,Fe)$_3$$AlSi_3O_{10}(F,OH)_2$; up to 25%–50%], and garnet [(Fe^{2+}, Ca^{2+}, Mg^{2+}, Mn^{2+})$_3$ (Fe^{3+}, Al^{3+}, Cr^{3+})$_2$ SiO_4; up to 5%–25%], despite the low concentration of xenotime [(Y, Th, U, Dy, Yb, Er, Gd) (PO_4)], occurring up at 1%–5%, this mineral is present in most samples (Table 1). From the NM, the most representative minerals are andalusite (Al_2SiO_5; up to 50%–75%), apatite [$Ca_5(PO_4)_3$(F, OH, Cl); up to 25%–50%], anatase (TiO_2; up to 25%–50%), zircon ($ZrSiO_4$; up to 5%–25%), rutile (TiO_2; up to 5%–25%), sillimanite (Al_2SiO_5; up to 5%–25%), and topaz [Al_2SiO_4(F,OH)$_2$; up to 5%–25%] (Table 1). It is important to note that cassiterite is possibly present as well, since some grains of this mineral were suspected of occurring in some nonmagnetic mineral fractions. Considering the total volume of the alluvial HM samples (MG + NM), the average abundances of ilmenite (50.15%) and tourmaline (11.36%) are highlighted in contrast with those from the other minerals that are all under 10%, such as biotite (8.55%), andalusite (5.52%), and others (<5%) (Table 2; Figure 3). The case of the REE- and other CRM-bearing minerals identified is described in the following sections, being the most significant or relatively abundant briefly characterized.

4.1.1 Rare earth element minerals

The dominant REE (-bearing) minerals identified in the samples are monazite (4.97%), xenotime (0.53%), zircon (2.58%), and apatite (4.14%), representing 12.23% of the sample volume (Table 2; Figure 3). Monazite and xenotime occur as fine hyaline grains, mostly with subhedral (to euhedral) habits and rounded shapes (Figure 4A), showing light yellow and green colors, respectively. Apatite occurs as

TABLE 2 Average mineral abundance values obtained by semi-quantitative analysis under binocular microscope for the 12 alluvial samples from Vale da Silveira, Castelo Branco region.

Mineral	Average (%)
Magnetic and paramagnetic	
Monazite	4.97
Xenotime	0.53
Sphene	0.03
Ilmenite	50.15
Epidote group	1.69
Tourmaline	11.36
Garnet	4.38
Leucoxene (MG)	0.16
Biotite	8.55
Iron oxy/hydroxides	0.59
Diamagnetic	
Apatite	4.14
Zircon	2.58
Rutile	0.75
Brookite	0.04
Anatase	3.10
Andalusite	5.52
Kyanite	0.02
Sillimanite	0.69
Topaz	0.54
Leucoxene (NM)	0.05
Muscovite	0.07
Scheelite	0.06
Cinnabar	0.04
Total	100.00

fine-medium anhedral grains showing clear signs of alteration, or as coarse subhedral–euhedral prismatic grains (Figure 4B). Zircon was identified in different crystal typologies, suggesting the predominance of those with prismatic face development. These zircon crystals range from colorless hyaline to semi-translucid orange–yellow and, in some cases, contain acicular or droplet-like (usually dark red) inclusions (Figure 4C).

4.1.2 Titanium minerals

The identified titanium minerals were ilmenite (50.15%), rutile (0.75%), anatase (3.10%), brookite (0.04%), sphene (0.03%), and leucoxene [MG (0.16%) and NM (0.05%)], at a total average of 54.28% of the sample volume (Table 2; Figure 3). The dominant Ti-bearing mineral, ilmenite, occurs as black grains with variable size and habit as (sub-)euhedral and in cases platy, tabular, granular, or irregular (Figure 4D).

4.1.3 Tungsten minerals

Scheelite was the only tungsten-bearing mineral identified and was present in very low average concentration (0.06%; Table 2 and Figure 3).

4.2 Geochemical characterization of alluvial heavy mineral concentrates

According to pXRF analysis (Table 3), the alluvial HM concentrates show high contents of Fe (up to 31.09%), Ti (up to 28.88%), Si (up to 13.57%), Ca (up to 9.10%), Al (up to 8.67%), P (up to 5.48%), K (up to 2.38%), Mn (up to 1.24%), and Zr (up to 207,018.13 mg/kg). In particular, the high Zr content in the NM has a strong influence on the minor elemental composition pattern (Figure 5A). Not considering Zr, the patterns of the elemental composition in the MG and NM have some similarities, highlighting the parallelism with V and Ti (Figures 5B and 6). However, some opposite behaviors of the pattern in relation to Mn and Fe in MG and Zr and minor Ca and P in NM contents are visible (Figures 5 and 6). The Σ(Ce, La, Nd, Pr) reaches 4,557.04 mg/kg, mostly based on the Σ(Ce, La, Nd) contents, because Pr is present in very low concentrations (Table 3; Figure 7). The Σ(Ce, La, Nd, Pr) and Th distributions show a very similar pattern, and in part, U and Pb distributions discreetly follow the other elements, overall, in MG (Figure 7). In the NM, the Zr content profile evidences a higher concentration and is followed by the U profile.

5 Discussion

The alluvial HM association analyzed is highly diversified and includes monazite, xenotime, ilmenite, epidote group minerals, tourmaline, garnet, magnetic leucoxene, biotite, iron oxides/hydroxides, sphene, apatite, zircon, rutile, brookite, anatase, andalusite, kyanite, sillimanite, topaz, non-magnetic leucoxene, muscovite, scheelite, cinnabar, and probably cassiterite. This mineral association incorporates the main HM identified by Antunes (2006) in petrographic studies of the CBM granitic rocks (see Section 1). The presence of alluvial biotite, muscovite, andalusite, and sillimanite, along with the abundant ilmenite and tourmaline, of the Al enriched biotite–muscovite granodiorite porphyry and two-mica granite is compatible with the description of Antunes (2006). Biotite, which according to Antunes (2006) and Antunes (2020) is one of the most abundant HM in the granitic rocks within the study area, is relatively poorly represented in the concentrates we studied and may also be poorly represented in relation to its actual presence in the alluvial deposits. Two main factors may account for the low recovery of biotite: a) its relatively low resistance to weathering and b) the sample treatment processes not being the most convenient for the physical and chemical characteristics of this mineral, thus causing it to being partially rejected. That is, the granularity of this mineral in the protolith rocks is much greater than that in which the alluvial samples were sieved (<3 mm), and its density may be lower

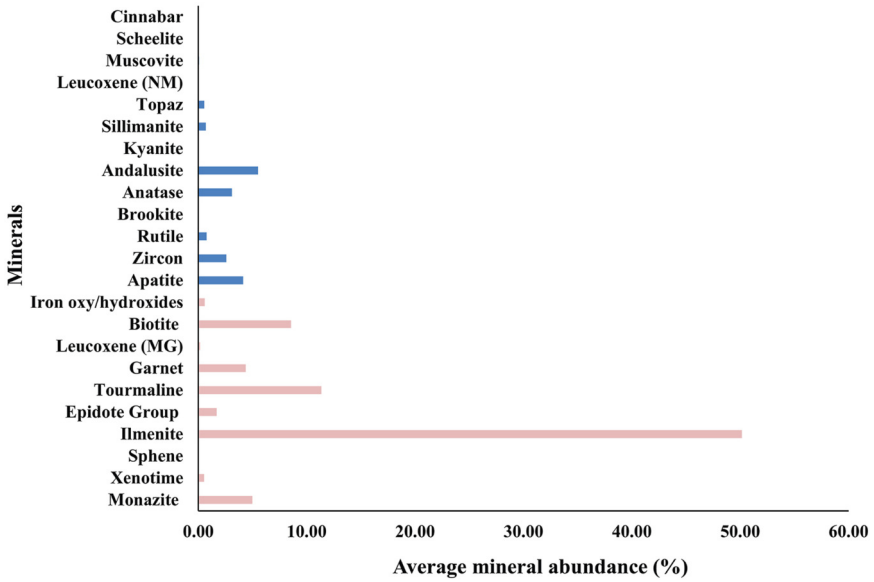

FIGURE 3
Average mineral abundance values obtained by semi-quantitative analysis under binocular microscope for the 12 alluvial samples from Vale da Silveira, Castelo Branco region. Blue denotes diamagnetic minerals, and pink denotes magnetic and paramagnetic minerals.

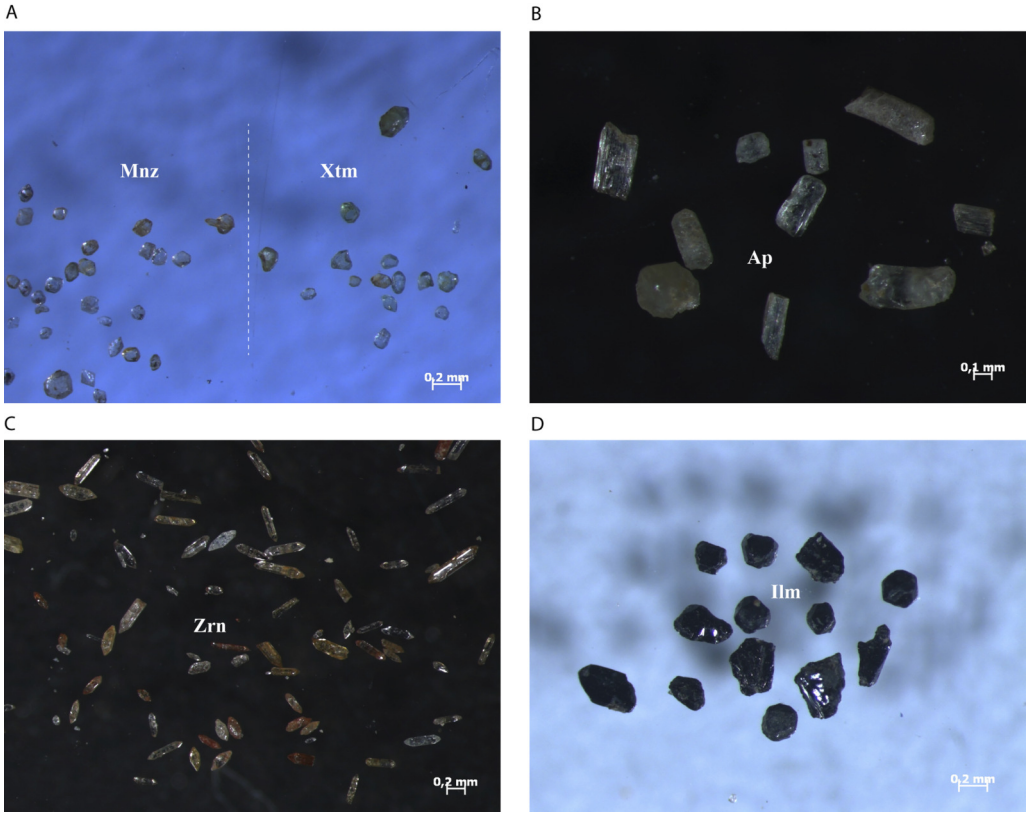

FIGURE 4
Alluvial REE minerals and ilmenite from Vale da Silveira (Castelo Branco) under binocular microscope: **(A)** monazite (Mnz; yellow hyaline, on the left) and xenotime (Xtm; green hyaline, on the right) grains; **(B)** apatite (Ap); **(C)** zircon (Zrn); **(D)** ilmenite (Ilm).

10.3389/fgeoc.2026.1766699

TABLE 3 Selected portable X-ray fluorescence results from bulk alluvial heavy mineral samples (average of eight measures). N.D.: not detected.

Sample	MG 660	MG 661	MG 662	MG 667	MG 668	MG 670	MG 681	MG 682	MG 689	MG 690–1	MG 690–2	MG 691
Weight (g)	7.89	10.43	4.15	25.2	32.77	24.68	1.38	6.3	9.94	22	8.54	19.16
(%)												
Mg	0.24	0.13	0.15	N.D.	0.02	0.04	0.20	N.D.	N.D.	N.D.	0.03	N.D.
Al	3.42	2.70	2.70	1.04	1.88	1.20	4.62	1.04	1.01	1.11	1.29	0.99
Si	4.89	3.91	4.19	1.64	2.93	1.85	7.40	1.71	1.60	1.86	2.20	1.61
Fe	29.14	28.79	27.16	30.32	29.91	30.38	30.09	30.45	29.19	30.51	30.10	31.09
P	0.49	0.49	0.57	0.21	0.21	0.33	0.28	0.27	0.28	0.18	0.20	0.24
K	0.89	0.63	0.38	0.20	0.42	0.24	1.27	0.27	0.20	0.20	0.23	0.20
Ca	0.62	0.51	0.42	0.14	0.20	0.13	0.28	0.15	0.10	0.10	0.13	0.16
Ti	19.64	22.17	22.92	26.79	24.61	25.78	15.24	26.42	25.68	26.64	26.27	26.50
Mn	0.94	0.94	0.88	1.24	1.09	1.23	0.62	1.22	1.15	1.07	1.03	1.12
(mg/kg)												
V	3,928.00	4,147.88	4,950.38	4,172.00	3,963.63	4,623.63	3,407.00	4,566.50	3,383.63	4,086.50	3,892.63	4,238.13
Cr	631.40	1,008.75	2,788.60	412.00	ND	969.43	324.00	532.00	552.50	ND	ND	345.00
Co	133.43	113.50	169.86	93.50	91.67	67.80	159.75	57.00	82.25	87.00	112.88	79.00
Ni	66.67	68.00	68.60	ND	ND	54.00	80.60	ND	ND	ND	ND	ND
Cu	48.67	84.75	98.00	40.00	54.00	49.25	46.00	ND	47.60	46.86	43.33	47.00
Zn	1,243.63	1,083.63	1,938.63	2,056.00	1,537.25	2,577.50	1,584.00	2,146.13	1,599.13	1,775.00	1,732.75	1,602.13
Ga	52.38	39.00	35.43	22.50	22.00	20.00	71.00	13.00	ND	ND	14.00	15.33
As	23.63	34.13	31.67	25.13	34.75	35.75	73.63	45.25	24.63	35.00	30.25	32.00
Rb	523.25	270.13	109.25	67.75	119.50	118.63	583.25	131.38	50.38	62.00	38.75	64.00
Y	154.88	150.38	379.38	88.75	37.25	251.25	39.00	126.88	181.50	61.00	52.13	96.00
Zr	2,280.25	4,239.88	3,613.13	2,916.25	2,117.88	3,194.00	1,859.13	2,261.25	2,237.75	2,171.13	2,323.38	2,082.50
Nb	792.13	1,011.88	1,173.63	1,180.63	1,094.00	1,218.88	651.13	1,010.00	1,050.88	1,299.50	1,339.50	1,140.13
Cd	30.29	25.29	37.00	20.50	17.83	28.17	29.14	30.25	19.67	14.80	13.14	22.80
Sn	188.29	163.00	184.67	ND	220.00	ND	163.00	152.00	60.00	ND	ND	ND
Sb	57.50	40.00	63.00	47.00	51.00	48.50	ND	91.00	45.00	51.00	43.00	44.00
La	292.63	507.75	1,083.13	363.50	185.13	733.38	150.38	446.50	463.13	226.88	182.88	179.88
Ce	583.13	1,056.00	2,098.63	743.75	369.25	1,447.13	281.63	954.86	881.88	443.00	391.13	366.00
Nd	332.88	568.88	1,080.00	447.88	266.75	702.50	209.71	441.00	476.50	300.75	253.50	246.29
Ta	159.25	179.75	168.71	108.75	129.13	84.50	168.13	84.00	88.63	104.63	124.00	119.50
Pb	55.63	42.43	137.63	20.40	24.33	209.13	18.25	244.50	36.63	34.38	43.50	36.86
Bi	72.13	84.75	83.75	108.38	89.25	111.75	55.63	106.88	107.38	107.13	92.63	101.13
Th	597.63	647.25	1,968.50	289.25	94.25	1,268.75	164.13	736.75	714.13	133.88	129.25	276.13
U	99.88	95.00	244.38	49.38	31.25	141.13	36.63	80.13	94.75	40.00	42.13	49.13
W	112.00	N.D.	N.D.	N.D.	N.D.	N.D.	N.D.	N.D.	N.D.	N.D.	N.D.	N.D.
Hg	81.63	78.13	66.38	69.38	67.75	87.50	81.13	69.50	57.25	61.63	50.50	62.88

(*Continued*)

TABLE 3 Continued

Sample	MG 660	MG 661	MG 662	MG 667	MG 668	MG 670	MG 681	MG 682	MG 689	MG 690–1	MG 690–2	MG 691
Pr	120.25	192.20	295.29	138.29	115.00	214.14	ND	200.75	133.50	114.00	111.67	110.67
La + Ce + Nd	1,208.63	2,132.63	4,261.75	1,555.13	821.13	2,883.00	641.71	1,842.36	1,821.50	970.63	827.50	792.16
La + Ce + Nd + Pr	1,328.88	2,324.83	4,557.04	1,693.41	936.13	3,097.14	641.71	2,043.11	1,955.00	1,084.63	939.17	902.83

Sample	NM 660	NM 661	NM 662	NM 667	NM 668	NM 670	NM 681	NM 682	NM 689	NM 690–1	NM 690–2	NM 691
Weight (g)	0.26	0.11	0.43	0.57	0.4	0.41	0.06	0.24	0.67	0.16	0.07	0.12
(%)												
Mg	N.D.	N.D.	N.D.	N.D.	N.D.	N.D.	N.D.	N.D.	N.D.	N.D.	N.D.	N.D.
Al	8.67	7.65	2.40	4.31	2.98	1.17	3.79	1.53	2.43	5.02	8.60	2.63
Si	13.57	10.57	6.48	8.84	12.86	6.52	9.61	7.06	7.27	10.56	10.37	6.62
Fe	1.39	1.41	1.45	1.82	0.76	1.17	2.53	1.10	1.06	1.25	2.19	0.96
P	4.99	4.33	3.04	3.83	5.29	5.01	3.66	5.26	5.48	2.89	2.28	3.33
K	2.03	1.07	0.63	1.43	2.38	0.62	1.72	0.65	0.50	1.57	1.33	0.71
Ca	8.16	4.18	1.84	2.61	2.96	0.88	9.10	3.87	2.50	2.07	4.28	1.75
Ti	6.63	15.39	28.88	20.45	9.18	18.67	21.72	21.28	20.22	22.50	21.71	27.25
Mn	0.14	0.07	0.05	0.04	0.03	0.01	0.18	0.06	0.04	0.03	0.08	0.04
(mg/kg)												
V	2,268.83	2,771.75	3,843.50	3,433.00	2,245.00	3,970.88	3,358.50	3,244.25	3,857.00	3,535.75	3,876.00	3,839.38
Cr	ND	325.00	379.00	395.25	366.00	1,678.75	373.67	349.00	1,159.13	429.25	406.00	383.00
Co	99.29	149.14	166.00	199.00	244.29	263.50	43.00	223.88	257.25	133.38	58.33	184.50
Ni	68.67	77.50	63.00	88.40	88.14	85.38	57.67	96.86	89.63	63.00	ND	74.14
Cu	277.88	345.13	439.75	413.25	547.13	680.50	78.00	600.88	572.38	315.50	74.63	432.50
Zn	79.00	72.00	53.75	190.88	70.00	ND	205.00	ND	58.00	73.75	354.63	47.00
Ga	71.63	50.57	62.50	51.38	32.00	ND	12.00	ND	14.67	27.38	73.50	20.50
As	106.71	152.38	167.13	182.88	256.88	275.75	32.25	326.29	213.38	134.75	32.75	190.75
Rb	186.00	131.63	74.75	221.38	195.25	116.50	166.63	85.63	89.88	147.75	136.50	81.38
Y	293.75	474.63	334.00	244.75	264.63	608.75	348.75	488.38	766.13	251.13	159.38	407.63
Zr	59,271.63	75,149.50	95,415.88	100,485.13	167,055.88	207,018.13	9,778.50	128,592.88	138,161.75	69,445.75	13,931.38	105,959.38
Nb	238.00	394.75	1,170.38	1,184.00	483.25	920.75	499.88	575.50	767.63	816.25	923.38	1,012.25
Cd	29.20	15.25	27.50	24.00	18.67	ND	ND	ND	18.00	11.00	ND	ND
Sn	351.75	152.00	206.14	1,878.00	2,912.25	1,477.13	284.67	660.88	739.00	673.13	247.40	5,122.38
Sb	59.60	57.50	55.80	108.50	134.50	121.00	ND	206.38	67.86	63.00	48.33	42.50
La	22.67	ND	62.75	52.75	18.00	161.57	77.13	34.00	309.13	44.83	34.50	56.50
Ce	ND	115.67	198.13	159.00	ND	451.88	185.63	124.00	757.88	150.20	ND	146.14
Nd	90.83	169.25	148.00	109.88	96.43	434.13	119.38	167.63	633.38	114.63	72.50	169.88
Ta	164.63	211.75	259.63	262.38	270.75	286.25	134.25	176.38	265.13	185.38	201.00	250.75
Pb	812.38	161.88	93.00	59.63	91.88	397.00	60.25	4,154.25	82.13	61.13	51.75	67.38

(*Continued*)

TABLE 3 Continued

Sample	NM 660	NM 661	NM 662	NM 667	NM 668	NM 670	NM 681	NM 682	NM 689	NM 690–1	NM 690–2	NM 691
Bi	66.38	92.88	139.75	144.75	159.25	236.88	25.00	147.88	188.13	113.13	25.25	149.88
Th	21.00	11.00	39.71	54.00	ND	925.25	111.13	ND	562.00	153.75	128.75	36.14
U	130.38	141.63	188.50	164.63	275.50	447.75	50.38	219.75	300.50	121.00	50.75	178.75
W	N.D.	59.67	36.00	46.50	81.00	196.13	138.75	231.13	79.71	356.75	488.75	139.00
Hg	107.88	123.88	103.00	166.88	160.50	217.25	77.63	153.88	153.88	206.13	132.25	188.88
Pr	ND	146.00	ND	ND	ND	173.00	ND	ND	208.17	ND	ND	ND
La + Ce + Nd	113.50	284.92	408.88	321.63	114.43	1,047.57	382.13	325.63	1,700.38	309.66	107.00	372.52
La + Ce + Nd + Pr	113.50	430.92	408.88	321.63	114.43	1,220.57	382.13	325.63	1,908.54	309.66	107.00	372.52

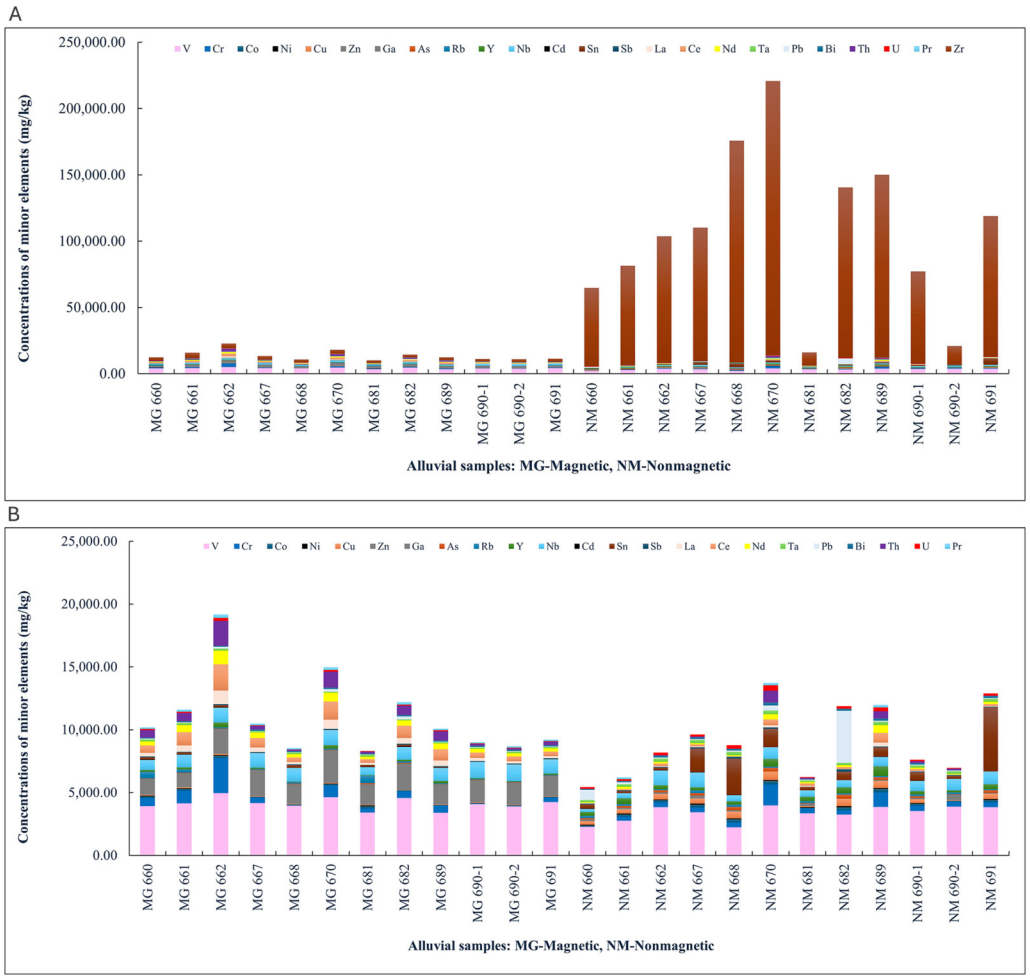

FIGURE 5
Distribution of minor element concentration obtained by pXRF analysis in MG and NM mineral fractions of alluvial HM samples **(A)** with Zr and **(B)** without Zr.

(2.7–3.3 g/cm^3; Mange and Maurer, 1992) relative to that of bromoform (2.89 g/cm^3) used in the mineral separation process. The latter assumption is supported by the fact that biotite grains have been observed floating in the heavy liquid during the mineral separation process. Thus, the incorporation of this mineral in the HM fraction could have been only promoted or facilitated by HM

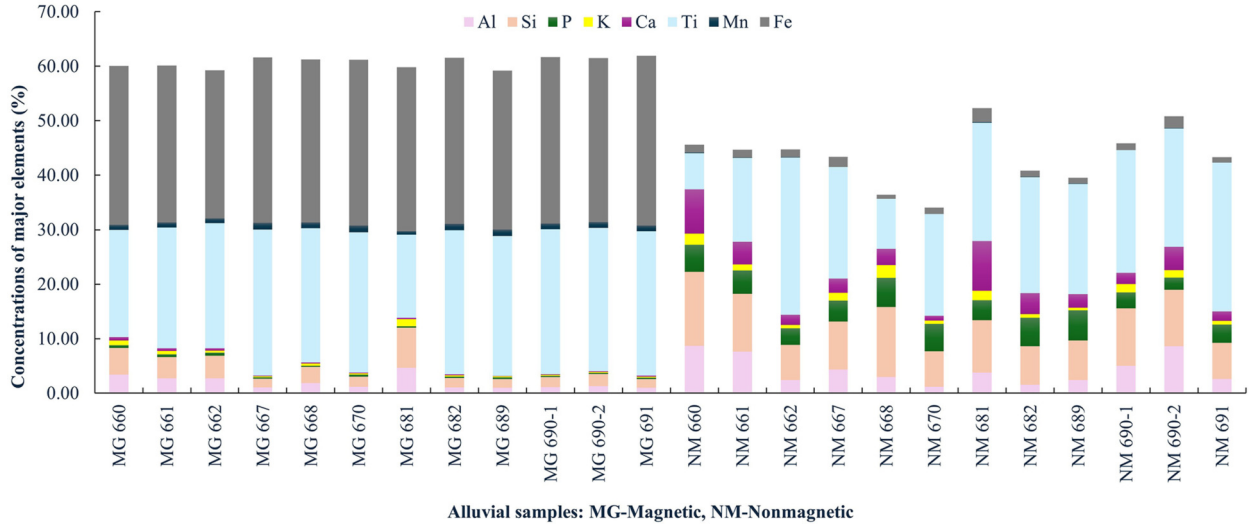

FIGURE 6
Distribution of major element concentration obtained by pXRF analysis in MG and NM mineral fraction of alluvial HM samples.

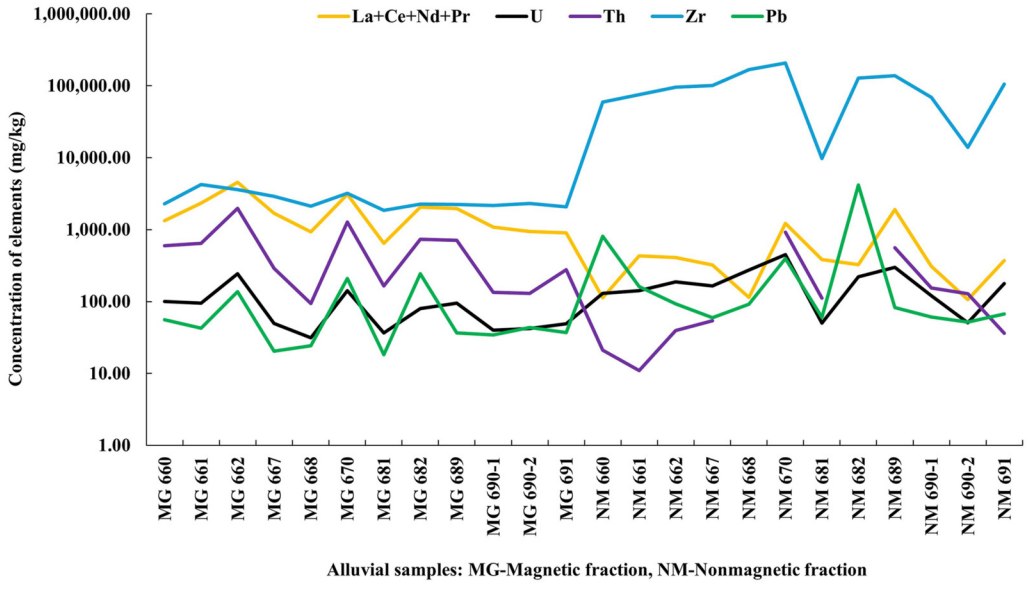

FIGURE 7
Detailed distribution of rare earth elements (ΣCe, La, Nd, Pr) and Th, U, Zr, and Pb obtained by pXRF analysis of alluvial HM samples.

inclusions (e.g., ilmenite, monazite, apatite, and xenotime) when present. Conversely, it is noteworthy that, to the best of our knowledge, certain minerals identified in the alluvial samples—such as xenotime, garnet, brookite, anatase, and cinnabar—have not been recorded in petrographic studies of the CBM granitic rocks or other lithologies previously described within this granitic context, perhaps because of its relative low representativeness in rock samples. It is possible that alluvial samples might include a minor local contribution from mineralized Sn–W quartz veins, metasedimentary xenoliths, or surmicaceous enclaves that were not recognized at the scale of existing geological mapping, owing to their limited spatial extent and negligible volumetric significance. Consequently, their influence on the present study is considered minimal. The mineralogical semi-quantitative analysis of alluvial HM samples performed under the binocular microscope is supported and compatible with the (pXRF) geochemical data obtained, and some correlations can be made, as presented below. The main alluvial Ti-bearing minerals are very well represented in the samples, especially ilmenite (average: 50.15%; Table 2 and Figure 3), justifying the predominance of Ti, along with Fe and Mn contents (Table 3; Figure 6). Other minerals hosting those elements, such as biotite, tourmaline, leucoxene (MG), and

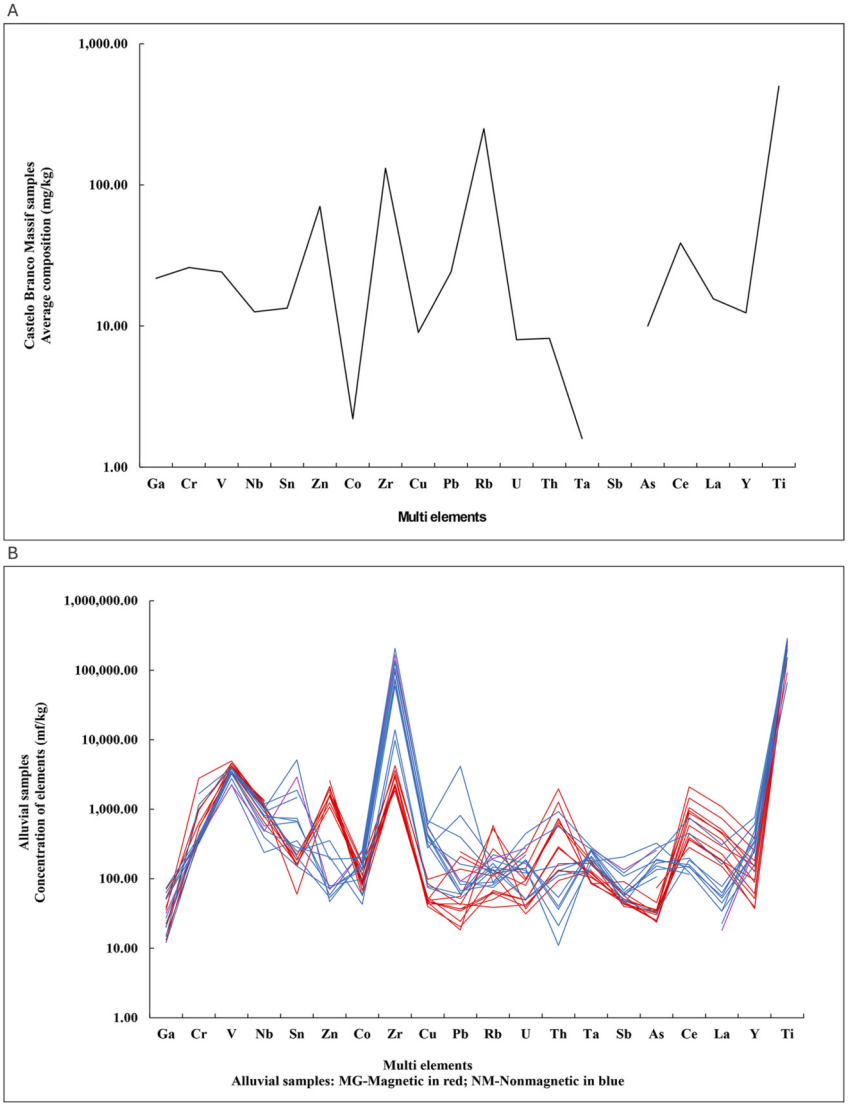

FIGURE 8
(A) Castelo Branco granitic rocks whole-rock average composition (data from Antunes, 2006). **(B)** Alluvial heavy mineral geochemical composition (red, magnetic mineral fraction; blue, nonmagnetic mineral fraction) by pXRF.

sphene in the MG mineral fraction and TiO_2 polymorphs and leucoxene (NM) in the NM fraction (Table 2; Figure 3) also reinforced these elements' high contents (Table 3; Figure 6). The higher contents of Ca and P in the NM mineral fraction (Table 3; Figure 6) are mainly due to the abundant presence of apatite (Table 2; Figure 3). In accordance with Bea (1996), approximately 70–95 wt% of REE (excluding Eu), Y, Th, and U contents in granite rocks, and particularly in peraluminous granites (as those from CBM), is part of the composition of the following (REE, Y, Th, U)-rich accessory minerals: monazite, xenotime (in the case of the low-Ca content of these granites), apatite, zircon, Th-orthosilicate, uraninite and betafite-pyrochlore. The relatively higher contents of La, Ce, Nd, Pr, and Th in the MG fraction (Table 3; Figure 7) may be justified by the monazite occurrence and partly by the less representative xenotime grains (having Y and minor LREE contents in their composition). The HM analysis carried out on alluvial samples indicated four main HM minerals (monazite, xenotime, zircon, and apatite), representing a relatively low average abundance of the samples (i.e., 12.23%), whose structure can include significant amounts of REE, which seems to be the main contributor of REE, Th, and U contents in the alluvial samples. According to Grácio et al. (2017), monazite from CBM rocks have higher REE content than zircon and probably higher modal abundance too. Consequently, they concluded that monazite may have a marked influence on the REE content of the granitic rocks, which is compatible with alluvial samples geochemical data. In addition, based on apatite geochemical data, Antunes (2006) interpreted low REE content on this mineral phase. Apart from Ce and La, monazite from CBM granitic facies, analyzed by Antunes (2006) and Antunes (2014), also contains high Th concentrations up to percentage level (i.e., 5,595 ± 112 to 64,369 ± 206 mg/kg), justifying the marked Th signature of the MG of the alluvial samples (Table 3; Figures 5 and 7). Moreover, monazite, along with apatite, xenotime, and zircon grains, may be less well

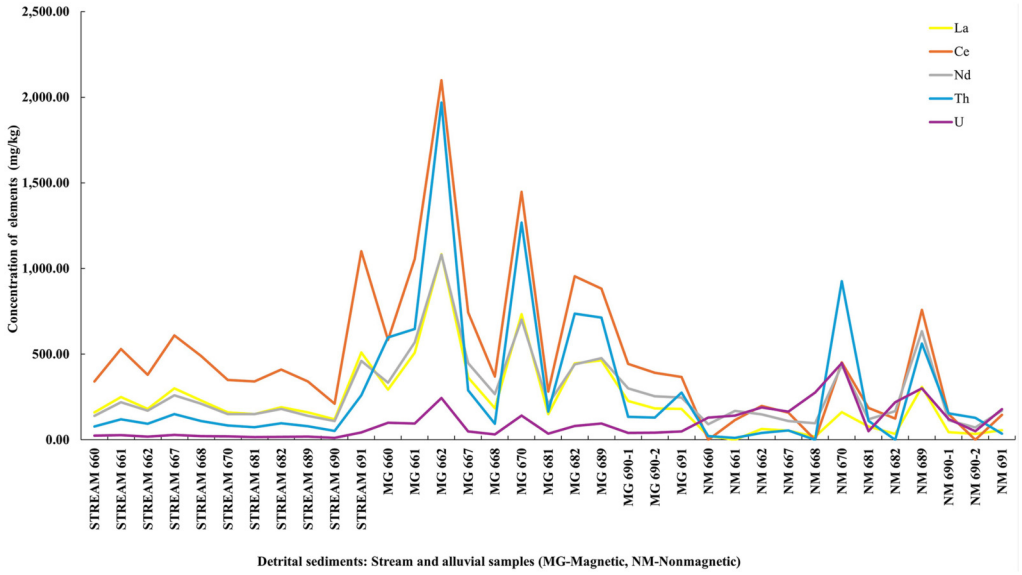

FIGURE 9
Stream sediments (INAA analysis; Inverno et al., 2007) and alluvial HM (pXRF analysis, this study): La, Ce, Nd, Th, and U concentration.

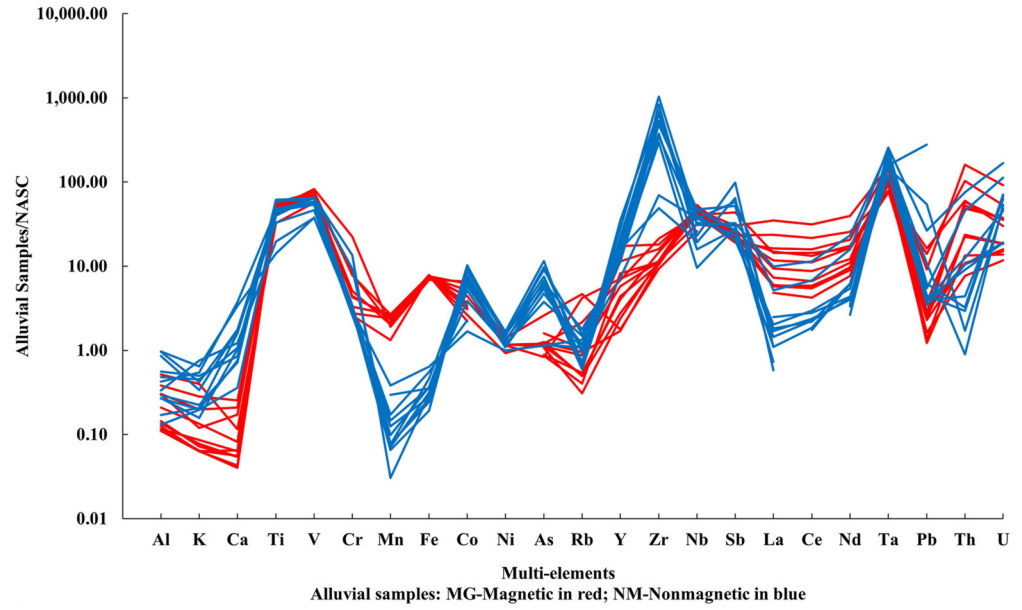

FIGURE 10
Alluvial heavy minerals element composition normalized to North American shale composite (NASC) (Gromet et al., 1984) plot (red, magnetic mineral fraction; blue, non-magnetic mineral fraction).

represented in the alluvial HM as free isolated grains because they can also occur unnoticed in analysis under the binocular microscope but are still included in biotite crystals, as in its original granitic source. Supporting this hypothesis is the relatively significant Zr content in the MG (Figures 5A, 8B), which can be an indication of some zircon included in biotite grains. High Zr and variable LREE, U, Y, and Pb contents are also represented in the NM geochemical fingerprint, mostly highlighting the influence of abundant free zircon grains and possibly that different crystal typologies have variable geochemical signatures (Figure 5).

In this same mineral fraction, the Al, K, and Si contents are also highlighted in relation to MG by the presence of sillimanite, andalusite, topaz, muscovite, and rare kyanite (Tables 2, 3; Figures 3, 6). There are significant Nb (up to 1,339.5 mg/kg) and Ta contents (up to 270.75 mg/kg) (Table 3; Figure 5). Despite the possible presence of other Nb-Ta bearing minerals not identified in

the present study, those elements can be associated with the occurrence of several minerals (Parker and Fleischer, 1968) in both mineral fractions of the alluvial samples, such as TiO_2 polymorphs, (possible) cassiterite, biotite, and ilmenite (Table 2; Figure 3). Additionally, the relative discrete values of W (up to 488.75 mg/kg), Hg (217.25 mg/kg), and Sn (5,122.38 mg/kg) can be correlated with the scarce occurrence of scheelite, cinnabar, and probably some unidentified cassiterite grains, respectively (Tables 2, 3; Figure 3).

In relation to the geochemical signature of the granitic rocks presented by Antunes (2006), there is an enrichment of most of the element's concentration in the alluvial HM samples, translated by the higher order of magnitude of the element's content (Figure 8). This is justified by the natural concentration of weathering-resistant heavy minerals, that carry those elements, trapped in the alluvial deposits and are then enhanced by different analytical techniques used and/or artificial mineral concentration in the laboratory (see Section 3 above). Despite this, alluvial HM samples and granitic rocks show parallel profiles, where in both, some elements have high or low concentration values in relation to their adjacent elements, suggesting a genetic correlation between them (Figure 8). This can be verified by the examples of the relatively higher concentration of trace elements such as Cr, V, Zr, Rb, Co, Ce, La, and Ti and lower values of Cu, Co, and Y in both patterns/profiles (Figure 8). The opposite behavior of the patterns/profiles regarding elemental enrichment or depletion reflects mainly the relative predominance of their host minerals in each of the mineral fractions (MG or NM), as explained above for Figure 5. The Σ(Ce, La) alluvial HM concentration has a higher order of magnitude (572.38–3,442.63 mg/kg) not just as their granitic source (average 54.4 mg/kg; Antunes, 2006) but also than NASC reference values (97.80 mg/kg; Gromet et al., 1984; Figure 10). Moreover, the geochemical signature of the alluvial HM samples also shows higher Σ(Ce, La) concentrations than their respective local stream sediments (330–1610 mg/kg by INAA; Inverno et al., 2007; Table 3; Figure 9), which is due to the natural concentration of HM in alluvia and during sample treatment. These stream sediments ΣREE (La, Ce, Nd, Sm, Eu, Tb, Yb, Lu) values (465.1–2,184.6 mg/kg; Inverno et al., 2007) are similar to their Σ(Ce, La, Nd) concentration values (440–2,070 mg/kg; Inverno et al., 2007) and are generally both lower than Σ(Ce, La, Nd) from the alluvial HM samples (e.g., MG: 641.71 to 4,261.75 mg/kg; Table 3). Hence, it can be inferred that the detrital minerals hosting the LREE are better represented than the HREE-containing minerals in those sediments' mineralogical association, which are compatible with the low abundance of xenotime in alluvial samples. Th (up to 1,969 mg/kg) in MG and U (up to 448 mg/kg) in NM (which includes apatite and zircon) are also higher than in granitic rocks (whole-rock average composition) and local stream sediments (Table 3; Figures 8, 9).

Considering the North American shale composite (NASC; Gromet et al., 1984) normalizing factors, the alluvial HM show enrichment in several elements (Ti, V, Fe, Co, Ni, As, Rb, Y, Zr, Nb, Sb, La, Ce, Nd, Ta, Pb, Th, and U), among which Ti, V, Y, Nb, Sb, La, Ce, Ta, W, Pb, Th, and U present concentrations 10× and above, and Zr (in NM) reaches 1000× (Figure 10). On the other hand, alluvial HM samples are relatively depleted in Al, K, Ca (in MG), and Mn (in NM).

As mentioned in Section 2, "Geological Setting," about the relatively higher concentration of Ti and REE and abundance of biotite that includes ilmenite and monazite (and xenotime) in middle CBM granitic facies (i.e., monzonitic granites, with sparse megacrystals, and porphyritic monzonitic granites), this seems to indicate the relatively higher potential of the CRM in the alluvium originating from these facies. Even so, the abundance of the alluvial REE minerals is relatively low in the studied alluvial samples sourced from monzonitic porphyritic granites that correspond to one of the most REE-enriched middle granitic facies of the CBM (Antunes, 2006; Antunes, 2020; Antunes et al., 2008). However, placer deposits elsewhere, including those formed in alluvial scenarios, have been relevant in providing REE through monazite and, more rarely, xenotime extraction as a coproduct of the recovery of industrial minerals such as ilmenite (Sengupta and Van Gosen, 2016)—highly abundant in CBM alluvial deposits.

6 Conclusion

The application of two complementary methodologies—(i) semiquantitative mineralogical analysis under a binocular microscope and (ii) chemical analysis using pXRF—enabled the rapid identification of a diverse heavy mineral assemblage and the geochemical fingerprint of alluvial samples from Vale da Silveira. The mineralogical and geochemical characteristics of these samples indicate a dominant provenance from the Castelo Branco granitic rocks. The samples exhibit relatively high concentrations of critical and strategic raw materials (e.g., Zr, Nb, Sb, La, Ce, Nd, Ta, Pb, Ti, Mn, and V). Among these, light REE and titanium are particularly significant, mainly hosted in monazite and ilmenite, respectively, and both in the magnetic heavy mineral fraction, the most abundant fraction, of the alluvial samples. Moreover, monazite, along with xenotime zircon and apatite, certainly contributes to the known REE, Th, and U anomalous values of the local stream sediments. The occurrence of monazite and ilmenite suggests potential for the formation of placer-type deposits sourced from the Castelo Branco granite, provided that the mineral grades, quality, and deposit volumes are sufficient for economic extraction. Notably, REE-bearing phases such as monazite and xenotime, as well as other industrial minerals, could potentially be recovered as coproducts of ilmenite. Considering the increasing demand for CRM, the Vale da Silveira area represents a potential site for further mineral investigation and potential small-scale exploitation of critical raw material-bearing alluvial deposits.

Data availability statement

The original contributions presented in the study are included in the article/Supplementary material; further inquiries can be directed to the corresponding author.

Author contributions

RS: Conceptualization, Data curation, Formal Analysis, Investigation, Methodology, Project administration, Resources, Software, Validation, Visualization, Writing – original draft, Writing – review and editing. TS: Conceptualization, Data curation, Formal Analysis, Investigation, Methodology, Resources, Software, Validation, Visualization, Writing – original draft,

Writing – review and editing. IM-M: Conceptualization, Data curation, Formal Analysis, Investigation, Methodology, Resources, Software, Validation, Visualization, Writing – original draft, Writing – review and editing. DO: Conceptualization, Data curation, Formal Analysis, Funding acquisition, Investigation, Methodology, Resources, Software, Validation, Visualization, Writing – original draft, Writing – review and editing. MB: Conceptualization, Data curation, Formal Analysis, Investigation, Methodology, Resources, Software, Validation, Visualization, Writing – original draft, Writing – review and editing. CI: Conceptualization, Data curation, Formal Analysis, Funding acquisition, Investigation, Methodology, Resources, Software, Validation, Visualization, Writing – original draft, Writing – review and editing.

Funding

The author(s) declared that financial support was received for this work and/or its publication. The present work was benefited from the project "Inventariação e prospecção de terras raras nas regiões fronteiriças da Beira Baixa e do Norte Alentejo," funded by the European Union Cross-Border INTERREG II program, and another project "Prospecção de Estanho e Volfrâmio e outros metais associados-Faixa Gois-Segura," funded by Portuguese funds, PIDDAC, for sample collection.

Acknowledgements

The authors thank the two reviewers for their constructive comments and recommendations which strengthened the present study.

Conflict of interest

The author(s) declared that this work was conducted in the absence of any commercial or financial relationships that could be construed as a potential conflict of interest.

Generative AI statement

The author(s) declared that generative AI was not used in the creation of this manuscript.

Any alternative text (alt text) provided alongside figures in this article has been generated by Frontiers with the support of artificial intelligence and reasonable efforts have been made to ensure accuracy, including review by the authors wherever possible. If you identify any issues, please contact us.

Publisher's note

Supplementary material

The Supplementary Material for this article can be found online at: https://www.frontiersin.org/articles/10.3389/fgeoc.2026.1766699/full#supplementary-material

References

Antunes, I. M. H. R. (2006). *Mineralogia, petrologia e geoquímica de rochas granitóides da área de Castelo-Branco-Idanha-a-Nova*. [dissertation/doctoral thesis]. [Coimbra]: University of Coimbra. Available online at: http://hdl.handle.net/10400.11/1140 (Accessed November 11, 2025).

Antunes, I. M. H. R. (2014). "Geochronology from the Castelo Branco pluton (Portugal) - isotopic methodologies," in *Geochronology - Methods and case studies* London: IntechOpen, 91–108. doi:10.5772/58686

Antunes, I. M. H. R. (2020). "As origens do Barrocal," in *Parque do Barrocal, 310 milhões de anos de construção* (Município Castelo Branco), 29–76.

Antunes, I. M. H. R., Neiva, A. M. R., Silva, M. M. V. G., and Corfu, F. (2008). Geochemistry of S-type granitic rocks from the reversely zoned Castelo Branco pluton (central Portugal). *Lithos* 103, 445–465. doi:10.1016/j.lithos.2007.10.003

Antunes, I. M. H. R., Neiva, A. M. R., and Silva, M. M. V. G. (2011). O plutão zonado de Castelo-Branco: geoquímica e petrogénese. O plutão zonado de Castelo Branco: geoquímica e petrogénese. *Congr. Ibérico Geoquímica, 8, Livro actas. Castelo Branco IPCB.* 1, 185–189.

Antunes, I. M. H. R., Albuquerque, M. T. D., and Sanches, F. A. N. (2014). Spatial risk assessment related to abandoned mining activities: an environmental management tool. *Environ. Earth Sci.* 72, 2631–2641. doi:10.1007/s12665-014-3170-4

Balaram, V. (2022). Rare Earth element deposits: sources, and exploration strategies. *J. Geol. Soc. India* 98, 1210–1216. doi:10.1007/s12594-022-2154-3

Bea, F. (1996). Residence of REE, Y, Th and U in granites and crustal photoliths: implications for the chemistry of crustal melts. *J. Petrol.* 37, 521–552. doi:10.1093/petrology/37.3.521

Charles, N., Tuduri, J., Lefebvre, G., Pourret, O., Gaillard, F., and Goodenough, K. (2023). "The rare Earth resources of Europe and Greenland mining potential and challenges," in *Metallic resources 1: geodynamic framework and remarkable examples in Europe* (Wiley), 1–142. doi:10.1002/9781394264810

European Commission (2021). "Directorate-general for internal market, industry, entrepreneurship and SMEs (2021)," in *3rd raw materials scoreboard – european innovation partnership on raw materials*. Luxembourg: Publications Office of the European Union. Available online at: https://data.europa.eu/doi/10.2873/567799 (Accessed November 11, 2025).

European Commission (2023). *Directorate-general for internal market, industry, entrepreneurship and SMEs, study on the critical raw materials for the EU 2023 – final report*. Luxembourg: Publications Office of the European Union. Available online at: https://data.europa.eu/doi/10.2873/725585 (Accessed November 11, 2025).

European Commission (2024). Regulation (Eu) 2024/1252 of the European parliament and of the council of 11 April 2024 establishing a framework for ensuring a secure and sustainable supply of critical raw materials and amending regulations (EU) no 168/2013, (EU) 2018/858, (EU) 2018/1724 and (EU) 2019/1020.

Gaspar, M., Grácio, N., Salgueiro, R., and Costa, M. (2022). Trace element geochemistry of alluvial TiO_2 polymorphs as a proxy for Sn and W deposits. *Mineral* 12 (10). doi:10.3390/min12101248

Goodenough, K. M., Schilling, J., Jonsson, E., Kalvig, P., Charles, N., Tuduri, J., et al. (2016). Europe's rare Earth element resource potential: an overview of REE metallogenetic provinces and their geodynamic setting. *Ore Geol. Rev.* 72 (1), 838–856. ISSN 0169-1368. doi:10.1016/j.oregeorev.2015.09.019

Grácio, N., Onken, C., Santos, R., Volongo, C., Antunes, I. M. H. R., and Ribeiro da Costa, I. (2017). Characterization of REE (+/- Ba)-bearing minerals from granitic rocks (central Portugal) and metasomatic rocks (Bayan Obo, China). *XII Congr. Nac. XI Iber. Geoquimica*, 12–15.

Gromet, L. P., Haskin, L. A., Korotev, R. L., and Dymek, R. F. (1984). The "North American shale composite": its compilation, major and trace element characteristics. *Geochim. Cosmochim. Acta* 48 (12), 2469–2482. doi:10.1016/0016-7037(84)90298-9

Iglesias, C., Antunes, I. M. H. R., Albuquerque, M. T. D., Martínez, J., and Taboada, J. (2020). Predicting ore content throughout a machine learning procedure – an Sn-W enrichment case study. *J. Geochem. Explor.* 208, 106405. 0375-6742. doi:10.1016/j.gexplo.2019.106405

Inverno, C. M. C., Oliveira, D. P. S., Viegas, L. F. S., Lencastre, J. P. B., and Salgueiro, R. (1998). "REE-Enriched Ordovician Quartzites in Vale de Cavalos, Portalegre, Portugal. Geocongress, T 98-Past achievements/Future challenges,". South Africa: Extended Abstracts, 153–157.*Geol. Soc.*

Inverno, C. M. C., Oliveira, D. P. S., Rodrigues, L., Viegas, L., Matos, J., Martins, L., et al. (2007). "Inventariação e prospecção de terras raras nas regiões fronteiriças da Beira Baixa e do Norte Alentejo," in *Internal report INETI*. Alfragide, 2982.

Lencastre, J. (1999). Estudo Preliminar da Monazite Nodular de Monfortinho, Portugal. *Estud. Notas Trab.* 42, 97–119.

Mange, A., and Maurer, H. F. W. (1992). *Heavy minerals in colour*. London: Chapman and Hall.

Morton, A. C. (1978). "Heavy minerals," in *Sedimentology, encyclopedia of Earth science* (Berlin, Heidelberg, Germany: Springer), 574–578.

Oliveira, J. T., Pereira, E., Ramalho, M., Antunes, M. T., and Monteiro, J. H. (1992). *Carta Geológica de Portugal na escala 1:500 000*. Lisboa: Serviços Geológicos de Portugal.

Parfenoff, A., Pomerol, C., and Tourenq, J. (1970). "Les minéraux en grains," in *Méthodes d'étude et détermination*. Paris: Masson et Cie.

Parker, R. L., and Fleischer, M. (1968). *Geochemistry of niobium and tantalum*. Washington, D. C.: USGS Publications.

Rosa, D., Salgueiro, R., Inverno, C., de Oliveira, D., and Guimarães, F. (2010). Occurrence and origin of alluvial xenotime from central Eastern Portugal (Central Iberian Zone/Ossa-Morena Zone). *Comum. Geol. (LNEG)* 97, 63–70.

Salgueiro, R., Rosa, D., Inverno, C., and de Oliveira, D. (2010). Ocorrência de xenótimo em amostras aluvionares da região centro-leste de Portugal (Zona Centro Ibérica/Zona de Ossa Morena). *VIII Congr. Nac. Geol. GEOTIC – Soc. Geol. Port. –Terra*. Available online at: http://e-terra.geopor.pt(1645-0388,20-n°11 (Accessed November 11, 2025).

Salgueiro, R., Rosa, D., Inverno, C., de Oliveira, D., Solá, A. R., and Guimarães, F. (2014). Alluvial xenotime and heavy minerals assemblage from the northern edge of Nisa-Albuquerque batholith, eastern Portugal: provenance and geochemical implications. *J. Geochem. Explor.* 146, 40–57. doi:10.1016/j.gexplo.2014.07.017

Salgueiro, R., Inverno, C., de Oliveira, D., and Guimarães, F. (2015). "New data on nodular monazite from Monfortinho (Idanha-a-Nova, Portugal)," in *Livro de Resumos do X Congresso Ibérico de Geoquímica/XVIII Semana de Geoquímica*, 147–150.

Salgueiro, R., Inverno, C., de Oliveira, D. P. S., Guimarães, F., Lencastre, J., and Rosa, D. (2020). Alluvial nodular monazite in Monfortinho (Idanha-a-Nova, Portugal): regional distribution and genesis. *J. Geochem. Explor.* 210, 106444. doi:10.1016/j.gexplo.2019.106444

Sanches, F., Roque, N., Antunes, I. M. R. H., and Albuquerque, T. (2012). "A geochemical Modelling approach in Lardosa region (Castelo Branco, Portugal): an environmental management tool,", 2012. Book of Abstracts, ISEG, 354. *9th Int. Symposium Environ. Geochem.l* Aveiro: Universidade de Aveiro.

Sengupta, D., and Van Gosen, B. (2016). Placer-type rare Earth element deposits. *Rev. Econ. Geol.* 18, 81–100. doi:10.1130/abs/2016AM-279551

SIORMINP (2025). SIORMINP -Sistema de Informação de Ocorrências e Recursos Minerais Portugueses. Available online at: https://geoportal.lneg.pt/pt/bds/siorminp#!/?substancia=0&district=0&council=0&dimension=0 (Accessed November 11, 2025).

Subasinghe, C. S., Ratnayake, A. S., Roser, B., Sudesh, M., Wijewardhana, D. U., Nishantha Attanayake, N., et al. (2022). Global distribution, genesis, exploitation, applications, production, and demand of industrial heavy minerals. *Arab. J. Geosci.* 15, 1616. doi:10.1007/s12517-022-10874-0